

RSC Advances



This is an *Accepted Manuscript*, which has been through the Royal Society of Chemistry peer review process and has been accepted for publication.

Accepted Manuscripts are published online shortly after acceptance, before technical editing, formatting and proof reading. Using this free service, authors can make their results available to the community, in citable form, before we publish the edited article. This *Accepted Manuscript* will be replaced by the edited, formatted and paginated article as soon as this is available.

You can find more information about *Accepted Manuscripts* in the [Information for Authors](#).

Please note that technical editing may introduce minor changes to the text and/or graphics, which may alter content. The journal's standard [Terms & Conditions](#) and the [Ethical guidelines](#) still apply. In no event shall the Royal Society of Chemistry be held responsible for any errors or omissions in this *Accepted Manuscript* or any consequences arising from the use of any information it contains.

Removal of methylene blue from waste water under low power irradiation source by Zn, Mn co-doped TiO₂ photocatalyst

Poonam Benjwal^a and Kamal K. Kar^{a, b, *}

^aAdvanced Nanoengineering Materials laboratory, Materials Science Programme,
Indian Institute of Technology Kanpur, Kanpur-208016, India,

^bAdvanced Nanoengineering Materials laboratory, Department of Mechanical Engineering,
Indian Institute of Technology Kanpur, Kanpur-208016, India

Email: kamalkk@iitk.ac.in, Fax # 0512-2597408, Phone # +91-512-2597687

*Corresponding author. Fax: +91 512 2597408; E-mail address: kamalkk@iitk.ac.in (Kamal K Kar)

Abstract

In present study a series of Zn, Mn co-doped titania (TiO₂) photocatalysts with varying dopant concentrations (0.0, 1.0 and 2.0 at.%) were synthesized via sol-gel process. The co-doped photocatalysts were characterized by XRD, XPS, SEM, TEM, Raman, FTIR and UV-Vis DRS techniques, where methylene blue was used as a probe environmental pollutant. The photocatalytic performances of the synthesized photocatalysts were evaluated under the very low (~2W) UV and visible power irradiation sources. Analysis of X-ray diffraction patterns suggests the multiphase structure of the photocatalyst while XPS results demonstrate that in co-doped TiO₂ the oxidation state of doped Zn metal ions is 2 (Zn²⁺), while Mn is in +2 and +3 (Mn^{2+/Mn³⁺}) state. The optical study results reveal the red shift in the co-doped samples, where with increasing co-dopant concentration the band gap is reduced. The highest photocatalytic degradation of MB is obtained with 1.0 at.% Zn, Mn co-doped TiO₂. This enhancement is attributed to the impurity levels introduced in band-gap and the high absorbance in UV region. The as-synthesized 1.0 at.% Zn, Mn co-doped TiO₂ provides a highest degradation efficiency (66.6 /watt×min) and thus may be practically used in the dyes removal process efficiently.

Keywords: Zn, Mn co-doping, TiO₂, photocatalysis, sol-gel, low power

1. Introduction

Recently, the heterogeneous catalysis has shown a great importance in many emerging fields such as power conversion and storage, removal of pollutants, synthesis of novel materials, etc [1-4]. Among these catalysis, the titania (TiO_2) based photocatalysts have attracted greater attention due to their high efficiency, nontoxicity, chemical inertness and high photostability [5, 6]. The photocatalytic activity of TiO_2 is based on the mechanism of the formation of electron/hole (e^-/h^+) pairs under the illumination of light. These radiation induced e^-/h^+ pairs initiate many chemical reactions by generating radical species on the surface of TiO_2 [7]. However, due to the high band gap ($E_g = 3.2$ eV), TiO_2 can be stimulated only by UV light, which comprises only 4% of the solar radiation [8]. Moreover, during photocatalysis, TiO_2 shows a low quantum efficiency with a high recombination rate of e^-/h^+ pairs, and thereby reduces its applicability as an efficient photocatalyzer [9]. Therefore, in order to maximize the photocatalytic activity of TiO_2 , it's essential to reduce its band-gap, which eventually results in enhancing its sensitivity in the visible range of solar radiation [10]. In view of this, a vast number of effective methods have been well explored in past, which includes the doping with various metals, nonmetals or coupling with semiconductors, etc. [11]. Among these, doping with transition metals reduces the recombination rate of photogenerated e^-/h^+ pairs in TiO_2 and thereby shifts the optical response from UV to visible spectral range [12-14]. These doped metal cations temporarily trap the charge carriers and thus reduce the recombination probability of e^-/h^+ pairs during the photocatalysis process. Recently, an approach to dope TiO_2 with more than one transitional metal ion has received much attention as it provides a finer control to the tuning of band-gap. Additionally, compared with single metal doping, it also improves photocatalytic activity of host material [15]. Zhi *et al.*

have observed that as compared to pure or single doped, an optimum amount of Zn-Fe co-doping into TiO₂ exhibits two folds improvement in the photocatalytic activity, which is attributed to the enriched electronic properties of TiO₂ by the co-dopants [16]. Another recent example have been demonstrated by Boningari *et al.* where they have studied the effect of different metals doping on the Mn doped TiO₂ for the investigation of catalytic reduction of NO with NH₃ [17]. The authors have found the maximum catalytic degradation with Ni/Mn doped TiO₂. It is found that the doping of transitional metals introduces new intrabands within the forbidden band gap of TiO₂, which thereby narrows the band gap and subsequently improves the optical absorption of TiO₂ in the UV and visible regions [18, 19]. Therefore, motivated by the need of improving the photocatalytic activity of TiO₂, here the co-doping of Zn, Mn in TiO₂ lattice is investigated. The transitional metal ions Zn and Mn are adopted as co-dopants due to their striking compatibility with TiO₂ for enhancing the photocatalytic activity [19-21]. Further, the control in the amount of co-dopant ions into TiO₂ lattice seems to be very important as it decides the effectiveness of the TiO₂ for photocatalysis applications. Thus, for optimization of the proper distribution of co-dopants ions in TiO₂, in present work the co-doping of Zn and Mn in varying concentration is carried out by simple sol-gel method as this process has been widely used for the incorporation of dopant into the TiO₂ lattice. Further, the effects of these co-dopants on the structural, optical and photocatalytic activity of TiO₂ in presence of UV as well as in visible light irradiation are inspected. Here, methylene blue (MB), an organic hazardous dye, is chosen as a model pollutant to explore the photocatalytic activity of TiO₂. Additionally, it is worth to mention that the photocatalytic activities of TiO₂ based photocatalysts have been studied by using high intensity irradiation sources, whose input powers varies between 20 to 1200 W. Use of such high power sources for the photocatalytic degradation is neither very energy efficient nor commercially

feasible. The catalytic performance using a very low intensity power source with intensity lower by at least two orders of magnitude has not been carried out to the best of our knowledge. In view of this, instead of using intense power sources, the present study considers the use of a 2W power source for the study of photocatalytic degradation.

2. Experimental

2.1 Materials and Method

Undoped and co-doped titanium oxide ($\text{Ti}_{1-2x}\text{Zn}_x\text{Mn}_x\text{O}_{2-2x}$) nanoparticles with $x = 0.00$ (undoped TiO_2), 0.01 and 0.02 (Zn, Mn co-doped TiO_2) were prepared by sol-gel process. Titanium tetraisobutoxide (TTIB; $\text{Ti}(\text{OC}_4\text{H}_9)_4$; Sigma-Aldrich), zinc nitrate ($\text{ZnNO}_3 \cdot 6\text{H}_2\text{O}$; Loba) and manganous nitrate ($\text{Mn}(\text{NO}_3)_2 \cdot 6\text{H}_2\text{O}$; Loba) were used as the TiO_2 , Zn and Mn precursors, respectively. Ethanol (Merck; 99%) was used as a solvent while HNO_3 (Fischer Scientific; 98%) served as the peptizing agent. A detailed method for preparing the TiO_2 nanoparticles is mentioned elsewhere [22]. In brief, 5 mL of TTIB was mixed with 12 mL of ethanol by vigorous stirring for 30 min to form solution A. Another solution (solution B) was prepared by mixing 0.9 mL HNO_3 with 10 mL ethanol and 5 mL deionized water using vigorous stirring for 30 min. Further, solution A was added drop wise to the solution B with a rate of 0.25 mL/min under vigorous magnetic stirring. After completion of mixing, the resultant solution was stirred further for 30 min and kept at room temperature for 24 h until the formation of a white gel. The prepared gel was dried at 100°C for 10 h to remove the volatile impurities and then grounded to obtain the powdered sample. Subsequently, further purification was carried out by centrifuging the powdered sample in ethanol for 2 h at 8000 rpm. Finally, the obtained powder was annealed at 500°C for 4 h. Zn, Mn co-doped TiO_2 ($x = 0.01$ and 0.02) powder was also prepared by similar

procedure. Here, another solution (solution C) was made by mixing desired amounts of $\text{ZnNO}_3 \cdot 6\text{H}_2\text{O}$ and $\text{Mn}(\text{NO}_3)_2 \cdot 6\text{H}_2\text{O}$ with 5 mL ethanol using vigorous stirring for 30 min. Subsequently, the solution C was added drop wise to the solution A to form a solution D, which was further added to the solution B drop wise with a rate of 0.25 mL/min. Proceeding steps were kept same as those used to prepare undoped TiO_2 . The co-doped TiO_2 was also annealed at 500°C . The description of the complete sol-gel experimental procedure is attached in the supplementary information (Fig. S1). Hence after, the annealed $\text{Ti}_{1-x}\text{Zn}_x\text{Mn}_x\text{O}_{2-x}$ with $x = 0.00$, 0.01 and 0.02 will be termed as TP0, TP1 and TP2, respectively. To compare the effect of co-doping over single doping, Zn or Mn doped TiO_2 samples, namely $\text{Ti}_{1-x}\text{Zn}_x\text{O}_{2-x}$ or $\text{Ti}_{1-x}\text{Mn}_x\text{O}_{2-x}$ with x values of 0.01 (Zn1, Mn1) and 0.02 (Zn2, Mn2) were also prepared by using the procedure similar to that adopted for co-doped photocatalysts.

2.2 Photocatalysts Characterization

The crystalline phase and variation in lattice constants of undoped and Zn, Mn co-doped TiO_2 were studied by X-ray diffraction (Bruker D8-Focus advance diffractometer) with $\text{Cu K}\alpha$ radiation of wavelength 1.5406 \AA in the range of 20 to 80° with a scanning rate of $1^\circ/\text{min}$. Surface morphology was examined by scanning electronic microscope (SEM, Model no- Zeiss EVO MA-15) as well as transmission electron microscopy (TEM, TECNAI T12, operating voltage 120V). The EDX elemental mapping of the photocatalyst was acquired by JEOL, (JSM-6010LA) SEM. The chemical states of the co-doped nanoparticles were evaluated by X-ray photoelectron spectra (XPS) acquired with a PHI5000 (Versa ProbiI, FEI Inc.) spectrometer using a monochromatic $\text{Al K}\alpha$ (1486.6 eV) source. Raman spectroscopy was performed by LabRam Micro-Raman spectrometer (Jobin-Yuon HR 800 UV) using a He-Ne (632.8 nm) laser excitation source. Fourier transform infrared spectroscopy (FTIR) was recorded (Bruker-FTIR)

by using KBr pallet in the range of 4000-400 cm^{-1} and UV-vis diffuse reflectance spectra (UV-vis DRS) spectral data were acquired in a (Varian Cary 500 Scan) UV-vis-NIR spectrophotometer having an integrating diffuse reflectance fixture in the range of 200 to 800 nm. The band gap of synthesized photocatalysts was calculated by using the Kubelka-Munk plots. The Photoluminescence spectra (PL) were measured by Edinburgh Fluorescence spectrophotometer (FLSP 920) in the range of 385-600 nm at room temperature.

2.3 Evolution of photocatalytic activity

The photocatalytic activities of the undoped, Zn, Mn and Zn, Mn co-doped TiO_2 were evaluated by using a 2 mM solution of MB in water as the active material. The photoactive $\text{Ti}_{1-x}\text{Zn}_x\text{Mn}_x\text{O}_{2-x}$ was dispersed in the MB solution, where the concentration of photocatalyst was kept 62 mM for each sample. Prior to photocatalytic experiment, the TiO_2 dispersed MB solution was magnetically stirred in the dark for 30 min to attain the adsorption/desorption equilibrium. Consequently, the above solution was irradiated with UV and/or visible light under constant magnetic stirring. Commercial light emitting diode based light sources were used for both UV ($\lambda \sim 360$ nm, 2W, Probtos LED) and visible light ($\lambda > 400$ nm, 2W, DPLED) photoreactors. The wavelengths of irradiation sources were measured by high-resolution spectrophotometer (HR 4000; Ocean optics) with a wavelength range of 200 to 1100 nm. To study the degradation of MB with irradiation time, a measured amount of irradiated solution was collected at selected irradiation interval of 0, 2, 4, 6, 8 and 10 h, respectively. Similar experiments were carried out with Zn, Mn co-doped TiO_2 . The photodegradation of MB was calculated by measuring the absorbance of the collected MB solutions by UV-vis spectrophotometer at $\lambda_{\text{max}} \sim 664$ nm. The photodegradation of MB was usually determined by $\frac{C_0 - C_t}{C_0} \times 100$, where C_0 (initial absorbance) and C_t are the concentrations of MB at time (0) and (t), respectively. Subsequently, the

photocatalytic activities of the photocatalyst were considered proportional to the relative degradation of MB.

3. Results and discussion

The phase structure and crystalline size of undoped and Zn, Mn co-doped TiO₂, annealed at 500°C, were investigated by X-ray diffraction. As shown in Fig. 1(A), multiphase TiO₂ shows a higher crystallinity with anatase as prevailing phase along with a small fraction of rutile and brookite. The XRD patterns of undoped and co-doped TiO₂ indicate that the increasing amount of Zn²⁺ and Mn²⁺ ions suppresses the formation of other phase (brookite and rutile). This may be probably because of the suppressed crystallization of brookite and rutile phases owing to the adsorption of Zn²⁺ and Mn²⁺ ions on the surface. Subsequently, TP1 and TP2 show a clear peak broadening, which indicate their small crystalline size than TP0. The crystalline size of phases in the synthesized photocatalysts was calculated by considering the FWHM values of anatase (200), rutile (110) and brookite (211) peaks (Table 1). The most intense peaks of anatase (101) and brookite (210) were not considered for calculation, as these peaks were overlapped. The crystalline sizes (D) were calculated by using the Scherrer formula given as $D = \frac{K\lambda}{\beta \cos\theta}$, where K is the shape factor (~0.9), λ is the X-ray wavelength (0.15418 nm), β is the full width at half maximum (FWHM) of the corresponding diffraction line and θ is the diffraction angle. It is worth noticing that no other phases such as Zn, Mn rich oxides (ZnMnTiO_x) are observed in the XRD patterns of the co-doped TiO₂. The absence of such phases might be due to small amount of co dopants. It also indicates that the co-dopants, i.e., Zn²⁺ and Mn²⁺ ions can replace Ti⁺⁴ from lattice sites (Fig.1D) [23]. In order to confirm the Zn, Mn co-doping and to evaluate their effect

on crystal structure, the lattice constants of undoped and co-doped TiO₂ were calculated by using the relations $d_{hkl} = \frac{\lambda}{2 \sin \theta}$ and $\frac{1}{d_{hkl}^2} = \frac{h^2+k^2}{a^2} + \frac{l^2}{c^2}$, where, d_{hkl} is the interplanar distance with miller indices h, k, and l while a and c are the lattice constants. Fig.1(B) shows the variation of lattice constants with different doping concentrations.

Table 1: Effect of co-doping concentration on average crystalline size

Samples	Crystalline size (nm)		
	Anatase	Rutile	Brookite
TP0	15	47	17
TP1	16	40	15
TP2	9	38	4

With increasing co-doping concentrations it is observed that, the lattice constant ‘ c ’ increases, while the lattice constant ‘ a ’ increases for TP1, however for TP2, its value decreases. The variations on the lattice constants values are related to the larger ionic radii of Zn⁺² (0.885 Å) and Mn⁺² (0.81 and 0.96 Å for low and high spins, respectively) as compare to that of Ti⁺⁴ (0.745 Å) [24]. Despite the large variation of ionic radii, Zn⁺² and Mn⁺² ions can replace the Ti⁺⁴ ions in TiO₂ as the Zn – O and Mn – O bond lengths of 1.93 [25] and ~2.03 Å [26] are comparable to the Ti – O bond lengths of 1.93 and 1.98 Å for the distorted octahedral [27]. The small variations of the order of 10⁻³ Å in the lattice parameters a and c of Zn, Mn co-doped TiO₂ are well justified with an average change of the order of 0.1 Å in the Zn – O and Mn – O bond lengths with a fractional doping of 0.01 and 0.02 (1.0 and 2.0 at.%) (order of change in lattice parameters (10⁻³ Å) = order of change in average bond length (0.1 Å) × atomic fraction of dopants (10⁻²)).

Hence, the variation of lattice constants (a and c) confirms that the Zn^{+2} and Mn^{+2} ions replace the Ti^{+4} sites. As, here the change along the “ c ” direction is more as compared to the “ a ” value, thus it can be said that Zn^{2+} and Mn^{2+} are substituting the Ti^{4+} mainly from bcc and fcc lattice position [28]. Moreover, the lattice strain in TiO_2 , which generates due to the incorporation of co-dopants was also calculated by using Williamson-Hall relation given as $\beta \cos\theta = \frac{0.9\lambda}{D} + 4\eta \sin\theta$, where η is the lattice strain [29]. The lattice strain values of all the photocatalyst were obtained from the slopes of the plot of $\beta \cos\theta$ versus $4\sin\theta$, which gives a straight line (Fig.2). The calculated lattice strain values for TP0, TP1, TP2 comes around 0.07, 0.49 and 0.31 respectively. Here, TP1 shows the high strain value than that of TP2, which may be due to the substitution of Ti^{4+} from TiO_2 lattice by co-dopants ions. Same types of results have been also reported by Thumber *et. al.*, where with increasing doping concentration, the lattice strain value decreases [30]. Thus, the obtained results show that TP1 contains smaller crystalline size with increasing antase phase as well as highest lattice strain, which indicates the easier uptake of co-dopants ions in TiO_2 lattice [31].

Further, to confirm the concrete presence of co-dopant and to evaluate their chemical states in TiO_2 XPS has been performed. Here to identify the difference due to the co-doping on TiO_2 chemical states XPS study was also carried out with pure and single Zn and Mn (Zn1, Mn1) doped TiO_2 . XPS spectra corresponding to O1s, Ti2p, Mn2p, and Zn2p peaks were analyzed by using XPSPEAK version 4.1 program where Shirley-typed background and Gaussian–Lorentzian (GL) distributions were used to fit the baselines and the XPS peaks, respectively. Fig. 3(a) shows the survey spectra of TP0, TP1 and TP2, which reveal the presence of Zn and Mn in co-doped samples. Though the amount of doping is less, but still the peaks related to co-dopants can be observed in the XPS graph. In TP0 (Fig. 3b), the high resolution spectrum of O1s reveals the

peaks at 528.61 and 529.69 eV, which can be assigned to the lattice oxygen (Ti-O) and to the surface hydroxyl group of TiO₂ (Ti-OH), respectively. In co-doped TiO₂, the XPS spectra of O1s displays a center peak with another peak at 530.03 eV, which indicates the presence of oxygen and surface bound Ti-OH group, respectively (Fig.3c,d). Here, the third peak (530.89 eV at TP1 and 531.33 eV at TP2) is due to the presence of Zn and Mn (Ti-O-Zn/Ti-O-Mn) bonds, which originates from the co-doping of Zn and Mn. Further, the higher binding energy of O in Ti-O-Zn/Ti-O-Mn bonds can be explained on the basis of electronegativity of co-dopants ions, as Zn (1.64) and Mn (1.55) contains higher electronegativity than Ti (1.54). Thus, the O in Ti-O-Zn/Ti-O-Mn is less negative (electron cloud is attracted more towards Zn and Mn) compared to that of O in Ti-O-Ti [18]. Fig. 3e shows the Ti2p spectra of the TP0, TP1 and TP2, where compared to the TP0, Ti2p spectra of TP1 and TP2 shifts towards lower binding energy (0.4 eV). This shifting can be attributed to the formation of oxygen vacancy on the surface of TiO₂. The energy difference between doublets of all Ti2p spectra is found around 5.5 eV, which clears that the core level Ti is in Ti⁴⁺ oxidation state. Fig. 3f shows the XPS spectra of the Mn2p core level of single Mn doped (Mn1) and co-doped TiO₂, where the peaks observed in the range of 640.6-652.4 eV, can be ascribed to the Mn 2p_{3/2} and Mn 2p_{1/2}. As, XPS signal for Mn²⁺ and Mn³⁺ are very close to each other (~640 eV), it can be concluded that the Mn is present in a mixed state, which is formed due to the substitution of Ti⁴⁺ ion from the TiO₂ lattice by Mn²⁺/Mn³⁺ ions. Fig.3g displays the high-resolution XPS spectra of single Zn doped (Zn1) and Zn, Mn co-doped TiO₂, which show the characteristics doublets of Zn2p in the range of 1020.9-1044.1 eV, with a spin orbit splitting of 23.2 eV, corresponding to the Zn²⁺ oxidation state [23]. Here, with increasing co-doping concentration the peaks shift towards higher binding energy, which is due to the formation of defects states in TiO₂.

The morphology of sol-gel synthesized undoped and co-doped TiO₂ was investigated by SEM and TEM techniques, where undoped as well as co-doped TiO₂ exhibit agglomerated surface having resemble flat flakes with rough morphology. The SEM micrographs (Fig. S2) reveal that the co-doping does not reflect any obvious influence on the morphology of the samples. The observed results indicate the rough morphology, which may be beneficial in case of adsorption of dye into the TiO₂ nanoparticles due to its high surface roughness as well as high surface area. Fig.4 shows the TEM micrographs of the photocatalysts, which further reveal the agglomerated nature of the sample. Fig. 4d shows the SAED pattern of TP0, indicating the polycrystalline nature of synthesized photocatalyst. As revealed from the XRD analysis (Table1), the crystalline size varies between 15 to 50 nm, thus the larger size particles observed in the SEM images are of polycrystalline nature. Further, to evaluate the distribution of Zn and Mn ions into TiO₂ matrix the EDX elemental mapping has been carried out. Fig.5 shows the elemental mapping of TP0, TP1 and TP2, which reveals that in TP1 and TP2 the Zn and Mn ions are firmly incorporated into the TiO₂.

The Raman spectra of TP0, TP1 and TP2 are depicted in Fig. 6. The Raman modes centered around 147, 200, and 642 cm⁻¹ are named as E_{g(1)}, E_{g(2)} and E_{g(3)} while two other modes at 401 and 522 cm⁻¹ are termed as B_{1g(1)} and B_{1g(2)} modes, respectively. These modes are the characteristic of anatase phase of TiO₂ [32]. The E_{g(1)} band is the strongest band found in the anatase phase of TiO₂. In addition, as the synthesized photocatalysts are polymorphic in nature, the weaker peaks between the region of 200-400 cm⁻¹ (247, 325 and 357 cm⁻¹) band are due to brookite and rutile phase of TiO₂ [33]. With increasing co-dopant concentrations, a slight red shift is observed in the E_{g(1)} and E_{g(2)} modes of co-doped photocatalyst (Fig 6.inset graph). This red shift is probably due to the incorporation of co-dopants into TiO₂ lattice. Thus, the obtained

frequencies of TP0, TP1 and TP2, annealed at 500°C, support the XRD results, which also suggest that the anatase is a predominant phase of sol-gel synthesized TiO₂.

To investigate the effect of Zn, Mn co-doping on the vibration of TiO₂ lattice, FTIR study was performed. Fig. 7 shows the FTIR spectra of the undoped and co-doped TiO₂, where the strong absorption bands at 487 and 561 cm⁻¹ might be due to Ti – O bond in the TiO₂ lattice. Further, a broad absorption band in the region of 3000-3500 cm⁻¹ is observed for both undoped and co-doped TiO₂, which can be assigned to the surface-bound hydroxyl groups and their stretching vibration on the surface of TiO₂ [34]. A second adsorption band at 1000-1700 cm⁻¹ is assigned to surface-adsorbed water molecules (H-O-H bending, peak at 1628 cm⁻¹) [35]. This confirms a strong interaction of water molecules towards TiO₂ surface, which forms a number of broad OH-stretching vibrations. A broad intense vibration region at 1000-1200 cm⁻¹ is credited to the Ti-O-Ti vibration. Further, the FTIR spectra of TP1 and TP2 photocatalysts show some additional peaks at the 2800-2900 cm⁻¹ region, which might be originated due to the formation of Zn/Mn-Ti-O bonds. Moreover, it is also noticed that the position of 724 cm⁻¹ band of TP0, which corresponds to the Ti-O vibrations shifts towards lower wavenumber with increasing co-dopant content. This can be explained that in co-doped TiO₂, Ti⁴⁺ ions are substituted by the co-dopant ions, thus forming oxygen vacancies to attain charge-neutrality. The absence of oxygen atoms in co-doped TiO₂ may reduce the Ti-O or newly form Zn/Mn-Ti-O bonds, which indicates the lowering of average force-constant value of chemical bonds [36]. Thus, in co-doped TiO₂ the peak corresponding to Ti-O bonds shifts to lower wavenumber. Therefore, FTIR analysis affirms that the incorporation of Zn, Mn ions in TiO₂ substitutes Ti⁴⁺ from lattice and creates oxygen vacancies.

The photocatalytic activity of TiO₂ is primarily related to its band-gap properties. Thus, to evaluate E_g value as well as electronic properties of the undoped and Zn, Mn co-doped TiO₂ the UV-vis spectrum, within the range of 200-800 nm wavelengths, is shown in Fig. 8(a), where TP0 shows a sharp absorption edge at about 402 nm (E_g ~3.1eV). With incorporation of co-dopant ions, the absorption edge is extended to the broader visible region (400~800 nm) and hence a red shift is observed in the co-doped TiO₂. This red shift in TP1 and TP2 is attributed to the impurity levels created by the Zn²⁺ and Mn²⁺ ions within the band gap of TiO₂. Due to the different valence states of Zn²⁺ and Mn²⁺ ions than the host metal ion (Ti⁴⁺) the oxygen deficiencies are generated in the co-doped TiO₂ [21]. Subsequently, the additional energy levels are created within the band gap of TiO₂. The incorporation of these extra energy levels is considered to be responsible for the apparent red shift in co-doped TiO₂. The E_g values of undoped and co-doped TiO₂ are evaluated from the plots of the square root of Kubelka-Munk function (αhv) against energy (hv). The relation between Kubelka-Munk function and energy is defined as $(\alpha hv)^{1/2} = A (hv - E_g)^m$, where, A is a constant, hv is the photon energy (E) with h being the Planck's constant (4.14 x 10⁻¹⁶ eV.s). The value of right side exponent (m) is taken to be 1/2 and 2 for indirect and direct band gap transitions, respectively. The calculated E_g value for the TP0, TP1, and TP2 comes around 3.1, 2.9 and 2.86 eV, respectively (Fig.8b, c, d). Thus, with increasing co-doping content, the band gap is reduced.

The photocatalytic activities of TP0, TP1 and TP2 were evaluated by the degradation of MB under UV and visible irradiation both (Fig. 9a, 9b), where TP0 has shown some visible photocatalytic activity for MB degradation. As due to high band gap (~ 3.2 eV) theoretically pristine TiO₂ can not absorb visible light, the visible photocatalytic activity of TP0 can be explained by TiO₂ photosensitization by MB dye molecules [37]. Here, the dye molecule can

inject its photo excited electrons into the conduction band of pristine TiO_2 , which initiate a number of redox chain of reactions. The MB pollutant can be completely degraded by these redox reactions. The whole mechanism of the visible light degradation of MB over TP0 has been provided into the supplementary information (S1; Fig.S3). The degradation of MB was also carried out in absence of photocatalyst (Blank), from where it is noticed that MB can degrade naturally, however the degradation rate is found to be extremely slow. Further, with both irradiation source, TP1 exhibits the maximum photocatalytic activity. There are many factors, which affect the photocatalytic activity of TiO_2 such as crystallinity, morphology and electronic properties. Thus, the increased photocatalytic activity of co-doped TiO_2 can be explained by considering the modification of these factors. It is evident that the polymorphic TiO_2 provides the synergistic effect. As in the present case the sol-gel synthesized TiO_2 consists of anatase/rutile/brookite phases, a possibility of heterojunction formation among these phases is possible. Thus, during the photocatalysis process the electron-hole pairs can be separated away due to the different crystalline structure and band gap values of the TiO_2 polymorphs [38]. Moreover, the diverse crystal structure of these phases might also play a critical role in the photocatalysis process, as it determines the adsorption of intermediate products, which form during the photocatalysis process. Further, during photocatalysis process holes produce hydroxyl radicals after reacting with the surface water, which is considered a dominant oxidant for the degradation of organic pollutant [39]. In case of TP1 and TP2, FTIR analysis shows that the incorporation of Zn and Mn ions produces the excess hydroxyl radicals. Nevertheless, in TP2, the decrease in the photocatalytic activity is possibly related to the excessive surface oxygen vacancies induced due to higher doping concentration [21]. The plausible mechanism of the photocatalytic activity of the synthesized photocatalysts can be explained by the energy band

gap structure of TiO_2 shown in Fig. 10. As TiO_2 has high E_g (3.2 eV), the direct excitation of electron from valance band (VB) to the conduction band (CB) in presence of visible light is not possible. On incorporation of Zn and Mn ions into TiO_2 lattice, the energy band gap of TiO_2 decreases due to the formation of impurity levels below CB in the band gap, where electrons can transfer from VB of TiO_2 to these energy levels. These electrons travel to surface and adsorbed by the O_2 and produce the $\bullet\text{O}_2$ ions, which can further converts to the strong redox species such as H_2O_2 and $\bullet\text{OH}$ ions [14]. These redox ions are responsible for the degradation of the surface adsorbed hazardous MB dye. In case of TP2, as Zn, Mn co-doping concentration increases, the density of new energy levels also increases, which ultimately enhances the recombination possibilities of electron and holes as they can be easily trapped on these recombination centers. Here due to the reduction of distances between the trapping sites, the increased recombination rate will compete with the photocatalytic redox process, which eventually slows down the photocatalytic rate [40]. Generally, to understand the mechanism of recombination of electron-hole pairs in semiconductors photoluminescence (PL) spectra is used, as PL emission arises due to the recombination of free charge carriers. Fig.11 illustrates the PL spectra of TiO_2 and Zn, Mn co-doped TiO_2 nanoparticles in the wavelength range of 385-600 nm, with an excitement wavelength of 355 nm. The PL spectra of photocatalysts show two main peaks around 414 and 434 nm, which can be attributed to the band-gap emission transmission and surface oxygen vacancies, respectively. In co-doped samples, lowering of the PL intensity can be associated with the transfer of electrons from excited TiO_2 to the new energy levels created by the co-dopant. As, PL emission generates due to the recombination of free charge carriers, the decreasing PL intensity of co-doped samples indicates the reduction in the recombination of electron and holes [41]. It is found that the PL emission intensity of TP2 is higher than that of TP1, indicating the

high recombination rate of charge carriers in TP2, which is probably the region of lower photocatalytic activity of TP2. Hence, though higher Zn, Mn co-doping narrows down the band gap, it fastens the recombination rate of e^-/h^+ pairs [42, 43]. Moreover, the photocatalytic activity of co-doped TiO₂ was also compared with single Zn/ Mn doped TiO₂ (Fig. S4), which shows that the co-doped TiO₂ provides higher degradation than that of single doped TiO₂. Besides of MB dye, the visible photocatalytic activity of the photocatalysts was also examined with a colorless pollutant using phenol. Fig. S5 shows the degradation of phenol with synthesized TP0, TP1 and TP2, which reveals that phenol could be degraded over TiO₂, however, due to a very good stability of this type of pollutant, the degradation rate was relatively lower, and after 10 h of visible irradiation, the maximum degradation rate was about 60% (TP1). Further, to evaluate the photocatalytic activity of co-doped TiO₂ with high power source, the photocatalytic experiments were also carried out with 450W visible light solar simulator (Oriel-Newport, Fig.S6). The obtained results reveal that with high irradiation power source, the co-doped TiO₂ (TP1) was able to degrade 90% of MB within 50 minutes. This implies that the as-synthesized photocatalysts can be efficiently used with high power sources, as well. The degradation of MB under UV and visible light irradiation follows the first-order kinetics. The reaction rate constants under UV and visible light irradiations (k_{UV} and k_{Vis}) are calculated from the slopes of the semi-log plots of concentration C/C_0 (Fig.12) using the Arrhenius equation $\ln \frac{C_t}{C_0} = -kt$, where, k represents the respective rate constants, k_{UV} or k_{Vis} for UV and visible irradiations, while C_t and C_0 are the concentrations of MB at time t and 0, respectively. For both types of irradiations (UV and visible), TP1 exhibits higher reaction rate constant (Table S1). Under UV irradiation, k_{UV} for TP0 is around 0.07, which, with the incorporation of 1.0 at. % Zn, Mn ions increases to a value of 0.13. This enhancement can be associated to the band-gap modification of TiO₂, which

improves the degradation of organic molecules of MB. The comparison of photocatalytic activities of Zn, Mn co-doped TiO₂ for UV and visible radiations is carried out further by correlating the photocatalytic rate constants for UV (k_{UV}) and visible (k_{Vis}) radiations to the absorbance (α_λ) $\lambda =$ at 300 and 700 nm, respectively. As shown in Fig. 13, the high correlation between α_λ and k values is observed for UV radiation, while the correlation for visible radiation remains poor. This suggests that for UV radiation the photoactivity is directly proportional to the number of the absorbed photons. On the other hand, for visible radiation with increasing dopant concentration k decreases despite increasing α_λ , which suggests a partial contribution of visible radiation photons in the photoactivity of the TiO₂ photocatalysts. The decreased photoactivity of TP2 as compared to TP1 for both UV and visible radiations can be attributed to the decreased values of α_λ in the UV region (Fig. 8a1). Furthermore, from the application point of view the synthesized photocatalyst should be stable [44]. Thus, the stability and reusability of these photocatalyst were examined by reusing the TP1 photocatalyst. For this, the TP0 photocatalyst was reused for four times (Fig.S7). After being used for four times, the dye degradation efficiency is found to be 70% in presence of visible light irradiation. This implies the good stability and reusability of the photocatalyst.

Apart from the structural parameters such as surface area, crystalline size and electronic properties, the photocatalytic activity of TiO₂ also depends on the irradiation source intensity (I_0). According to the Fermi-Golden rule transition probability is proportional to the density of final states (ρ_f), i.e., the density of available states in CB. Again, under continuous illumination with a light source of fixed photon energies, the fraction of occupied states ($\delta\rho_f$) in the CB is proportional to the I_0 . Hence, the effective density of final states ($\rho_f - \delta\rho_f$) decreases with increasing I_0 , which consequently decreases the transition probability. Thus, the numbers of

transition do not increase linearly with increasing I_0 but effectively decreasing the photocatalytic degradation per unit I_0 . To compare the photocatalytic activity of studies conducted using sources with varying intensity, the degradation efficiency per unit power (Φ) can be defined as $\Phi = S/(L_0 t) \times 10^{-5}$, where S is the % degradation at time t (min) and L_0 is the power rating of the illumination source in watt (W). Using the above formula, a comparison has been made with the as synthesized photocatalyst (TP1) to the literature reported values, which suggests that the application of low power source enhances the degradation efficiency severally (Table S2). It is evident from Table S2 that with low intensity visible irradiation source (2W) the Zn, Mn co doped TiO₂ provides high degradation efficiency of $\sim 66.6 \text{ W}^{-1} \text{ min}^{-1}$ as compared to $\sim 37.5 \text{ W}^{-1} \text{ min}^{-1}$ for N doped TiO₂ [45].

4. Conclusions

Undoped and Zn, Mn co-doped TiO₂ photocatalysts were synthesized by sol-gel method and their photocatalytic activity for the degradation of MB under UV and visible irradiation were evaluated. Analysis of XRD pattern shows the formation of polymorphic TiO₂, where with increasing doping antase phase increases. The XPS analysis confirms the co-doping of Zn and Mn in the TiO₂. Furthermore, the band gap of TiO₂ exhibits a red shift with increasing dopant concentration. Though 2.0 at. % Zn, Mn co-doped TiO₂ (TP2) shows the highest red shift, the maximum photocatalytic activity is observed for 1.0 at. % (TP1) dopant concentration under both UV as well as visible light irradiations. This enhanced photocatalytic degradation by TP1 is attributed to its multiphase structure and increased absorption in UV range as well as the efficient transfer of electron hole pairs through co-dopant ions in the sub energy bands of TiO₂.

With low intensity visible irradiation source (2W), the 1.0 at. % Zn, Mn co-doped TiO₂ provides a very high degradation of $\sim 66.6 \text{ W}^{-1} \times \text{min}^{-1}$. Thus, due to the striking features, the as-synthesized Zn, Mn co-doped TiO₂ can be efficiently used for the removal of organic pollutants.

Acknowledgements

The authors acknowledge the financial support provided by Department of Science and Technology, India for carrying out this research work.

References

- [1] S. Liu, Z.-R. Tang, Y. Sun, J. C. Colmenares and Y.-J. Xu, *Chem. Soc. Rev.*, 2015, **44**, 5053-5075.
- [2] R. Sharma and K. K. Kar, *Electrochim. Acta*, 2015, **156**, 199-206.
- [3] C. Han, M.-Q. Yang, B. Weng and Y.-J. Xu, *Phys. Chem. Chem. Phys.*, 2014, **16**, 16891-16903.
- [4] N. Zhang, M.-Q. Yang, S. Liu, Y. Sun and Y.-J. Xu, *Chem. Rev.*, 2015, **115**, 10307-10377.
- [5] H. Zhang, G. Chen and D. W. Bahnemann, *J. Mater. Chem.*, 2009, **19**, 5089-5121.
- [6] P. Benjwal and K. K. Kar, *J. Environ. Chem. Eng.*, 2015, **3**, 2076-2083.
- [7] W. He, Z. Fang, K. Zhang, X. Li, D. Ji, X. Jiang, C. Qiu and K. Guo, *RSC Adv.*, 2015, **5**, 54853-54860.
- [8] X. Li, Z. Guo and T. He, *Phys. Chem. Chem. Phys.*, 2013, **15**, 20037-20045.
- [9] A. A. Ismail and D. W. Bahnemann, *J. Mater. Chem.*, 2011, **21**, 11686-11707.
- [10] S. S. Boxi and S. Paria, *RSC Adv.*, 2015, **5**, 37657-37668.
- [11] Y. Zhang, Z.-R. Tang, X. Fu and Y.-J. Xu, *ACS Nano*, 2010, **4**, 7303-7314.

- [12] J. Choi, H. Park and M. R. Hoffmann, *J. Phys. Chem. C*, 2009, **114**, 783-792.
- [13] W. J. Foo, C. Zhang and G. W. Ho, *Nanoscale*, 2013, **5**, 759-764.
- [14] A. Ajmal, I. Majeed, R. N. Malik, H. Idriss and M. A. Nadeem, *RSC Adv.*, 2014, **4**, 37003-37026.
- [15] V. Jabbari, M. Hamadani, A. Reisi-Vanani, P. Razi, S. Hoseinifard and D. Villagran, *RSC Adv.*, 2015,
- [16] Z.-h. Yuan, J.-h. Jia and L.-d. Zhang, *Mater. Chem. Phys.*, 2002, **73**, 323-326.
- [17] B. Thirupathi and P. G. Smirniotis, *Appl. Catal., B*, 2011, **110**, 195-206.
- [18] P. Benjwal and K. K. Kar, *Mater. Chem. Phys.*, 2015, **160**, 279-288.
- [19] Q. R. Deng, X. H. Xia, M. L. Guo, Y. Gao and G. Shao, *Mater. Lett.*, 2011, **65**, 2051-2054.
- [20] L. Jing, B. Xin, F. Yuan, L. Xue, B. Wang and H. Fu, *J. Phys. Chem. B*, 2006, **110**, 17860-17865.
- [21] Y. Zhao, C. Li, X. Liu, F. Gu, H. Du and L. Shi, *Appl. Catal., B*, 2008, **79**, 208-215.
- [22] X. Zhang and Q. Liu, *Mater. Lett.*, 2008, **62**, 2589-2592.
- [23] M. E. Fragalà, I. Cacciotti, Y. Aleeva, R. L. Nigro, A. Bianco, G. Malandrino, C. Spinella, G. Pezzotti and G. Gusmano, *CrystEngComm*, 2010, **12**, 3858-3865.
- [24] R. D. Shannon and C. T. Prewitt, *Acta Cryst.*, 1969, **B25**, 925-946.
- [25] B. Xiang, P. Wang, X. Zhang, S. A. Dayeh, D. P. R. Aplin, C. Soci, D. Yu and D. Wang, *Nano Lett.*, 2007, **7**, 323-328.
- [26] Z. V. Saponjic, N. M. Dimitrijevic, O. G. Poluektov, L. X. Chen, E. Wasinger, U. Welp, D. M. Tiede, X. Zuo and T. Rajh, *J. Phys. Chem. B*, 2006, **110**, 25441-25450.
- [27] J. Muscat, V. Swamy and N. M. Harrison, *Phys. Rev. B*, 2002, **65**, 224112.

- [28] A. Burns, G. Hayes, W. Li, J. Hirvonen, J. D. Demaree and S. I. Shah, *Mater. Sci. Eng., B*, 2004, **111**, 150-155.
- [29] B. Prasad, C. Ghosh, A. Chakraborty, N. Bandyopadhyay and R. K. Ray, *Desalination*, 2011, **274**, 105-112.
- [30] A. Thurber, K. Reddy, V. Shutthanandan, M. H. Engelhard, C. Wang, J. Hays and A. Punnoose, *Phys. Rev. B*, 2007, **76**, 165206.
- [31] D. Chen, Z. Jiang, J. Geng, Q. Wang and D. Yang, *Ind. Eng. Chem. Res.*, 2007, **46**, 2741-2746.
- [32] X. Chen and S. S. Mao, *Chem. Rev.*, 2007, **107**, 2891-2959.
- [33] G. A. Tompsett, G. A. Bowmaker, R. P. Cooney, J. B. Metson, K. A. Rodgers and J. M. Seakins, *J. Raman Spectrosc.*, 1995, **26**, 57-62.
- [34] R. Sharma and K. K. Kar, *J. Mater. Chem. A*, 2015, **3**, 11948-11959.
- [35] W.-C. Hung, S.-H. Fu, J.-J. Tseng, H. Chu and T.-H. Ko, *Chemosphere*, 2007, **66**, 2142-2151.
- [36] M. Koelsch, S. Cassaignon, J. Guillemoles and J. Jolivet, *Thin Solid Films*, 2002, **403**, 312-319.
- [37] J. Zhang, J. Xi and Z. Ji, *J. Mater. Chem.*, 2012, **22**, 17700-17708.
- [38] Y. Liao, W. Que, Q. Jia, Y. He, J. Zhang and P. Zhong, *J. Mater. Chem.*, 2012, **22**, 7937-7944.
- [39] E. Neyens and J. Baeyens, *J. Hazard. Mater.*, 2003, **98**, 33-50.
- [40] J. Zhu, F. Chen, J. Zhang, H. Chen and M. Anpo, *J Photochem Photobiol A. Chem.*, 2006, **180**, 196-204.

- [41] B. Chai, T. Peng, X. Zhang, J. Mao, K. Li and X. Zhang, *Dalton Trans.*, 2013, **42**, 3402-3409.
- [42] Y. Cong, J. Zhang, F. Chen, M. Anpo and D. He, *J. Phys. Chem. C*, 2007, **111**, 10618-10623.
- [43] S. Rehman, R. Ullah, A. M. Butt and N. D. Gohar, *J. Hazard. Mater.*, 2009, **170**, 560-569.
- [44] P. Benjwal, M. Kumar, P. Chamoli and K. K. Kar, *RSC Adv.*, 2015, **5**, 73249-73260.
- [45] Y. Zhao, X. Qiu and C. Burda, *Chem. Mater.*, 2008, **20**, 2629-2636.

Figures with Captions

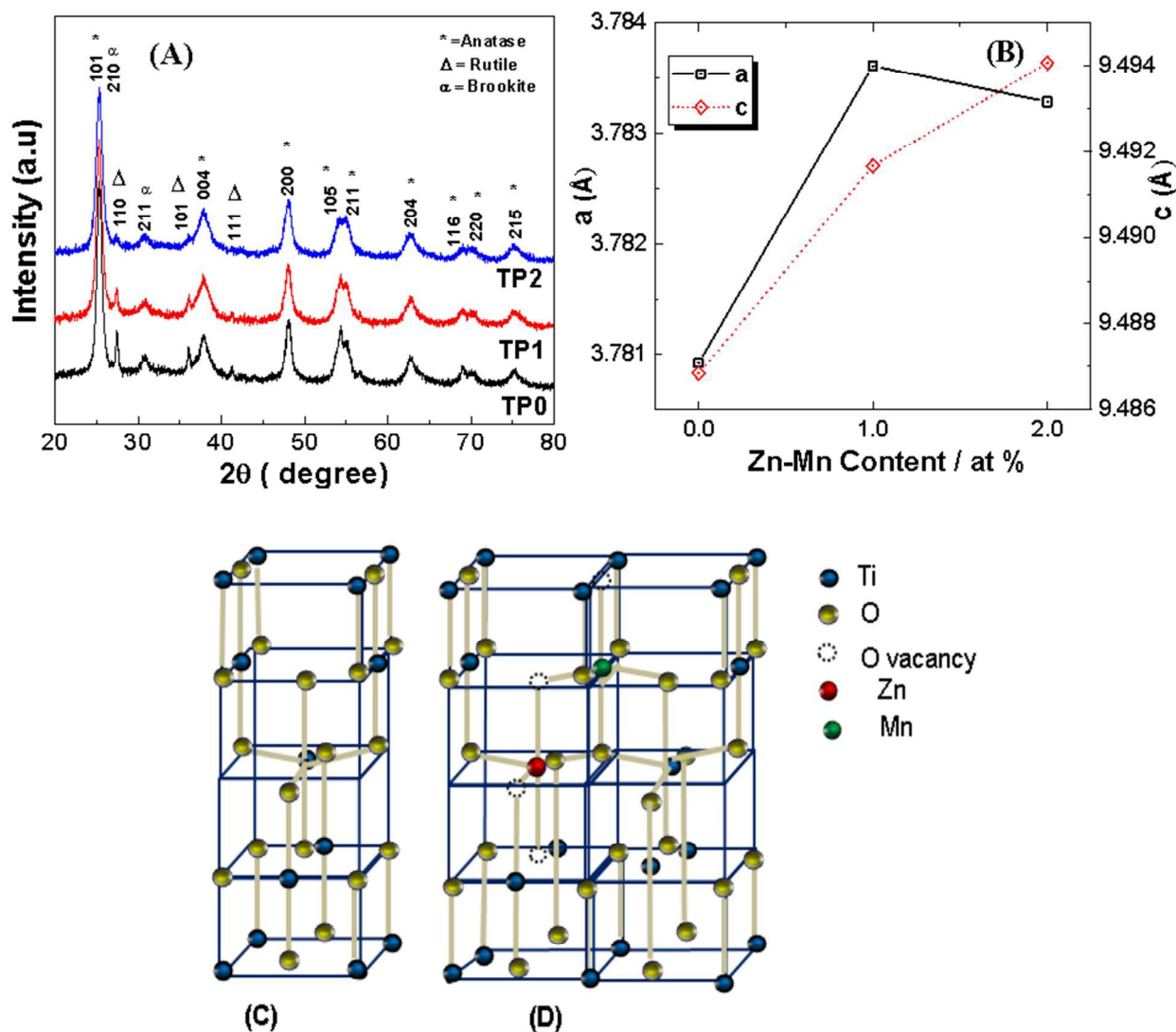


Fig. 1. (A) X-ray diffraction pattern of TP0, TP1 and TP2, and (B) variation in lattice constants with varying Zn, Mn co-doping concentrations. Schematic showing (C) the unit cell of anatase TiO₂ and (D) insertion of Zn²⁺ and Mn²⁺ replace Ti⁴⁺ ions from the lattice and create oxygen vacancies.

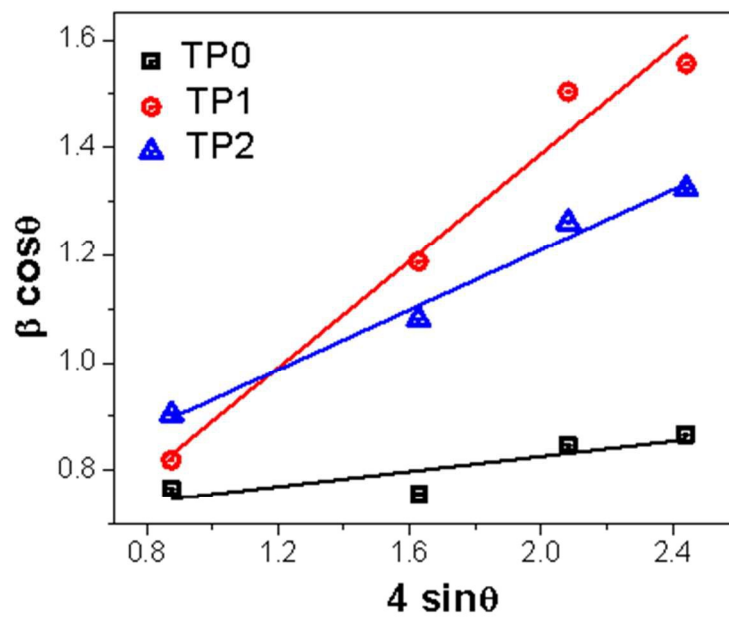


Fig. 2. Williamson–Hall ($\beta \cos \theta$ versus $4 \sin \theta$) plot for synthesized photocatalysts.

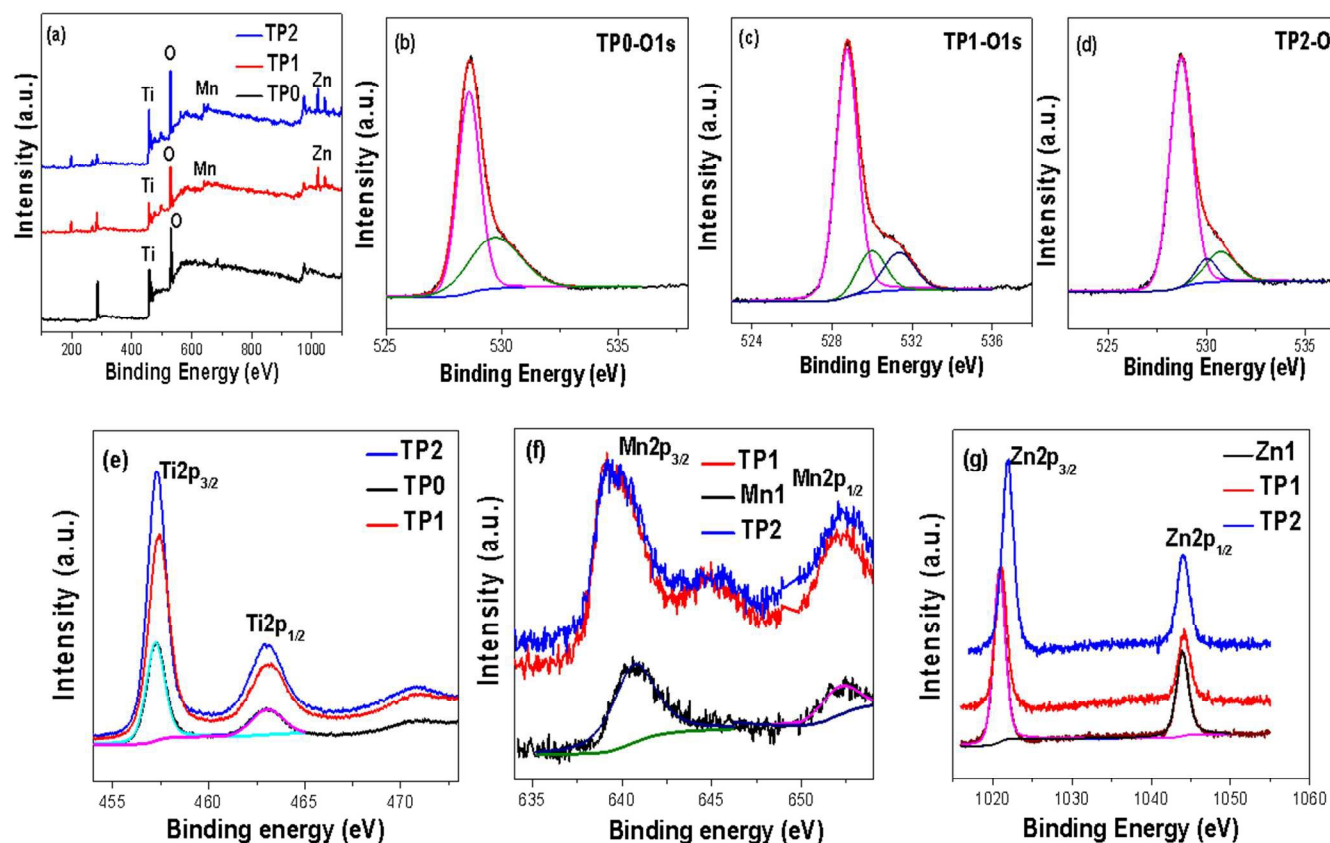


Fig. 3. (a) XPS survey scan of TP0, TP1 and TP2, which reveals the presence of Zn and Mn in co-doped samples. The O1s high resolution spectra of (b) TP0, (c) TP1 and (d) TP2. (e) Ti2p high resolution spectra of TP0, TP1 and TP2. (f) Mn2p spectra of TP1, TP2 and Mn1. (g) Zn2p spectra of TP1, TP2 and Zn1.

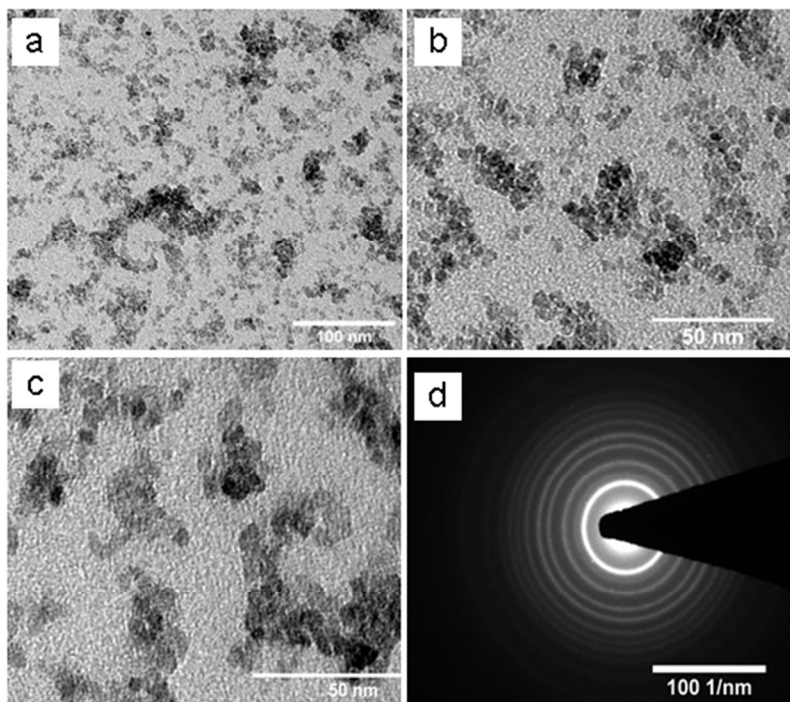


Fig. 4. TEM image of (a) TP0, (b) TP1, (c) TP2 and (d) SAED pattern of TP0.

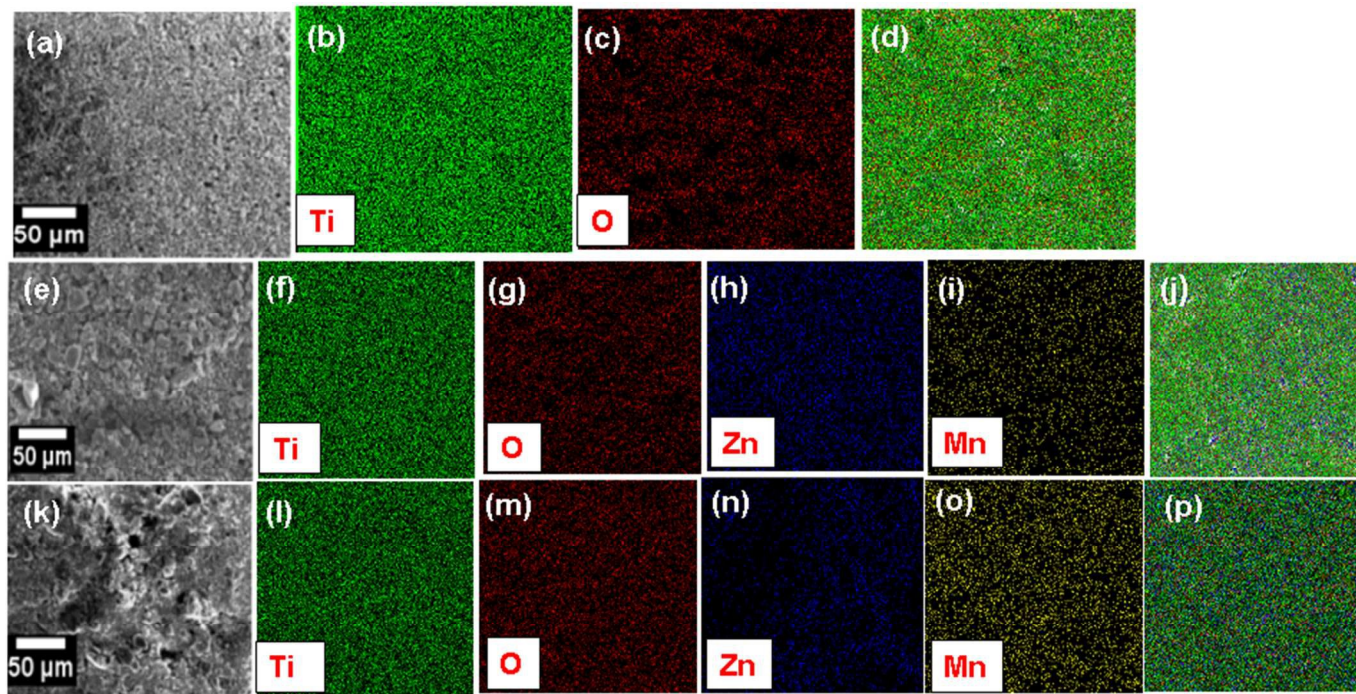


Fig. 5. EDX elemental mapping of undoped and co-doped TiO_2 nanoparticles. SEM micrograph of (a) TP0, (e) TP1 and (k) TP2. Elemental mapping, showing the presence of (b) Ti and (c) O in TP0, (f) Ti, (g) O, (h) Zn and (i) Mn in TP1, (l) Ti, (m) O, (n) Zn and (o) Mn in TP2, respectively. Here (d), (i) and (p) are showing the combined elemental mapping images of TP0, TP1 and TP2, revealing the distribution of Zn, Mn, Ti and O in TiO_2 matrix, respectively.

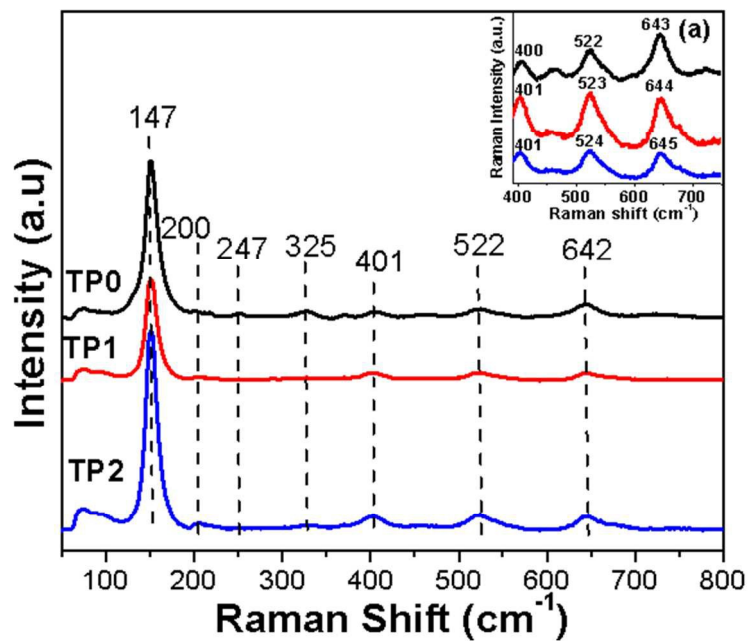


Fig. 6. Raman spectra of undoped and co-doped TiO_2 calcined at 500°C for 4 hours. (a) Inset shows the enlarged magnified view of Raman spectra in $400\text{--}700\text{ cm}^{-1}$ range.

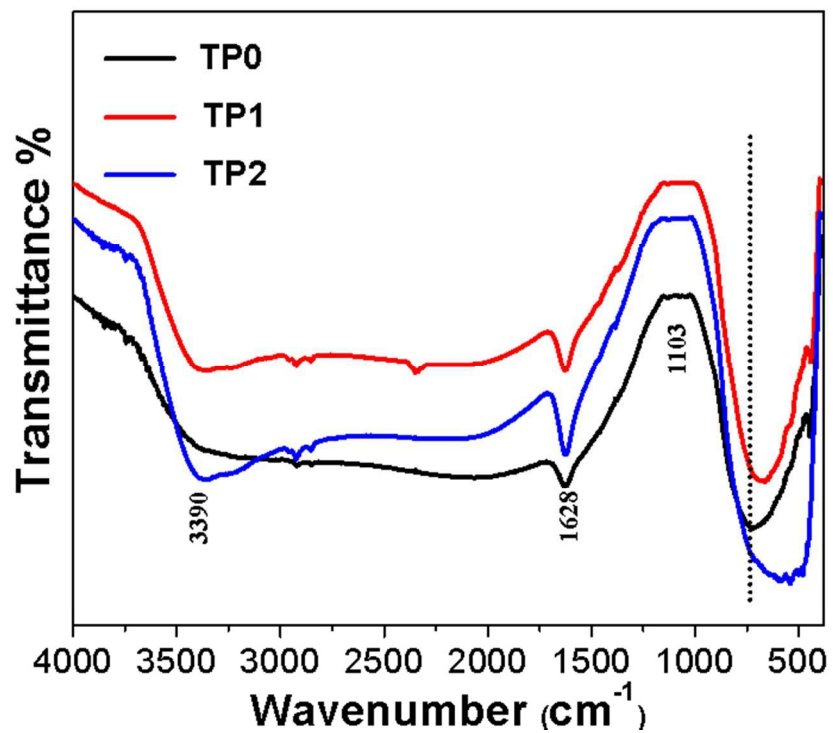


Fig. 7. FTIR of undoped and Zn, Mn co-doped TiO₂.

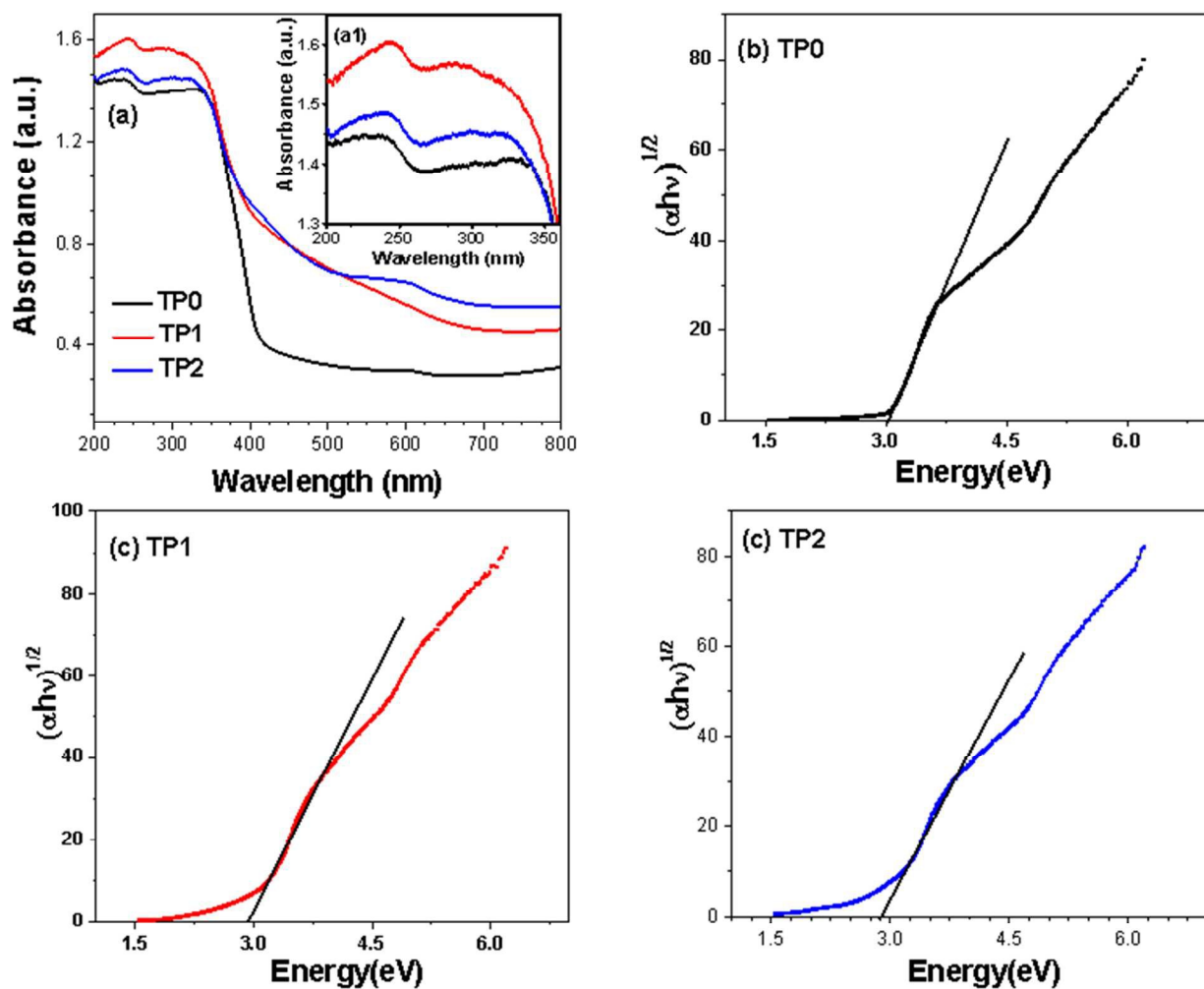


Fig. 8(a) Optical absorbance of undoped and co-doped TiO₂, where inset (a1) shows the absorption behavior in UV region. Kubelka-Munk function plot for band gap calculation of (b) TP0, (c) TP1 and (c) TP2. The lines define the E_g values.

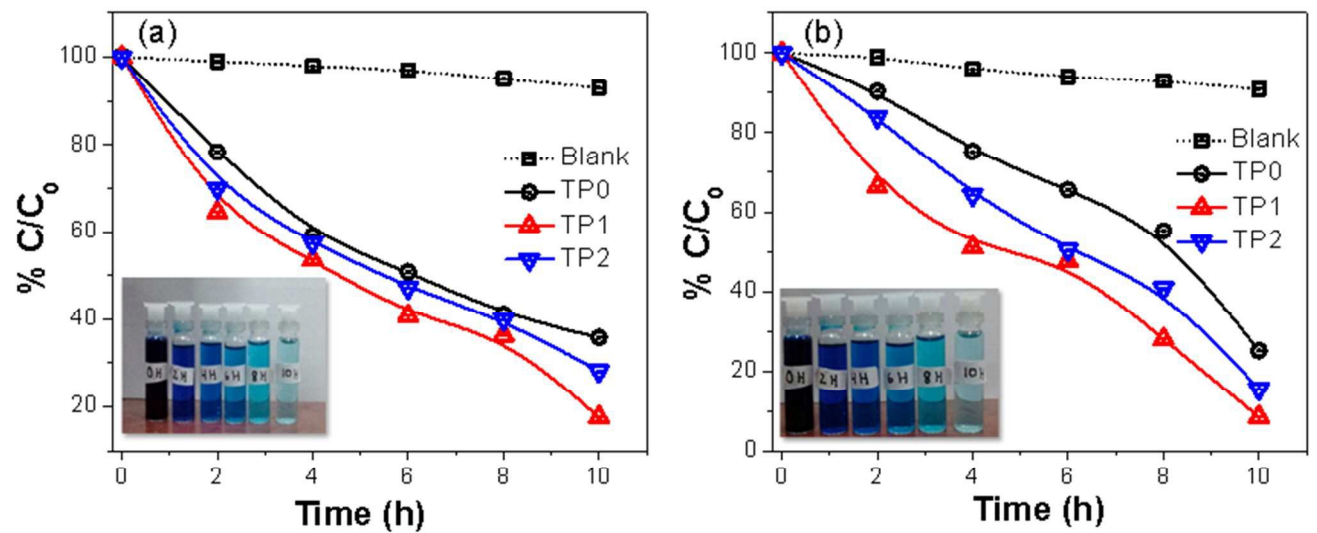


Fig. 9. Comparison of relative concentration of undoped and co-doped TiO₂ under the presence of (a) visible light and (b) UV light, where the dashed lines show the degradation of MB in absence (Blank) of photocatalyst. The insets image of (a) and (b) show the degradation of MB by TP1 in presence of visible and UV irradiation, respectively.

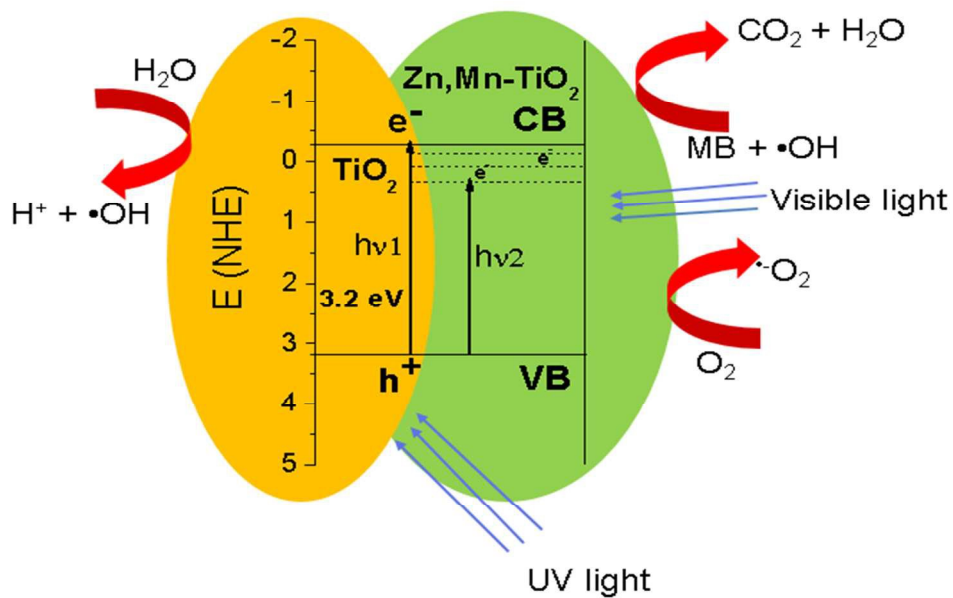


Fig. 10. Plausible mechanism of the MB degradation by Zn, Mn co-doped TiO_2 where $h\nu_1$ and $h\nu_2$ denotes the transition from CB to VB by pristine TiO_2 and Zn, Mn co-doped TiO_2 respectively.

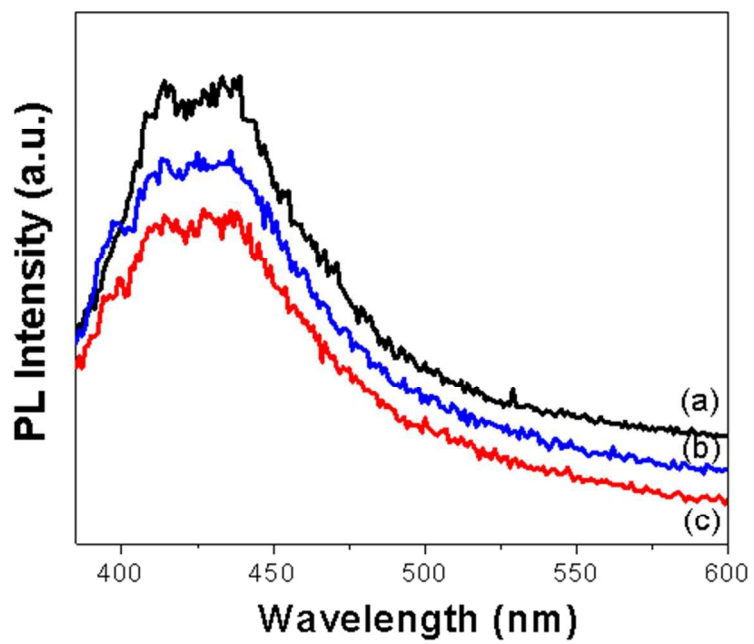


Fig. 11. PL spectra of the (a) TP0, (b) TP2 and (c) TP1.

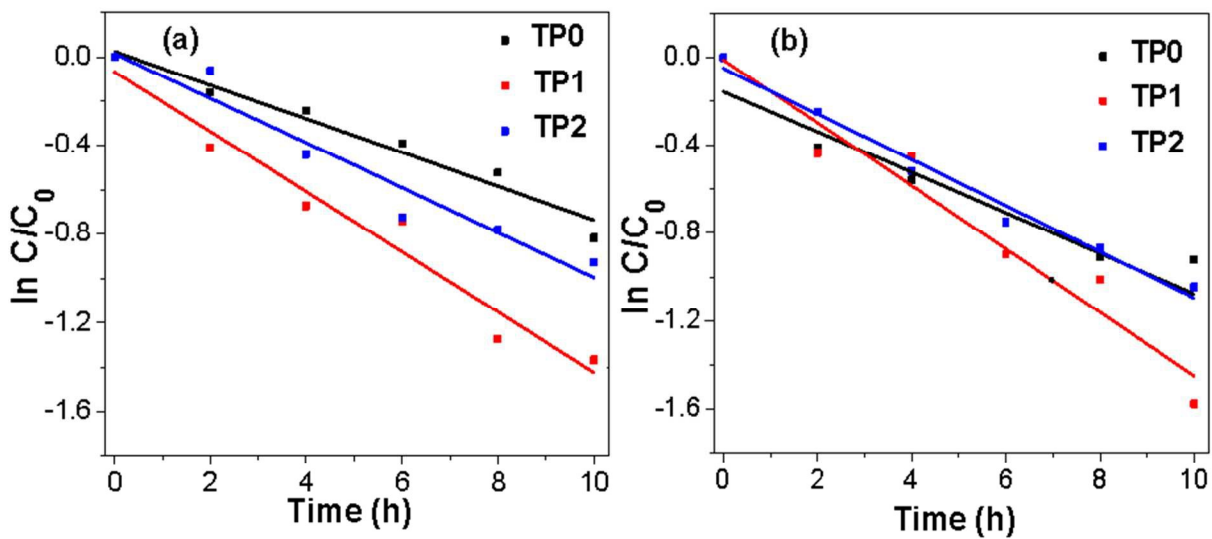


Fig. 12. Variation of log plots of relative concentrations of undoped and co-doped TiO_2 with time for the calculation of rate constant (a) UV light and (b) visible light irradiation.

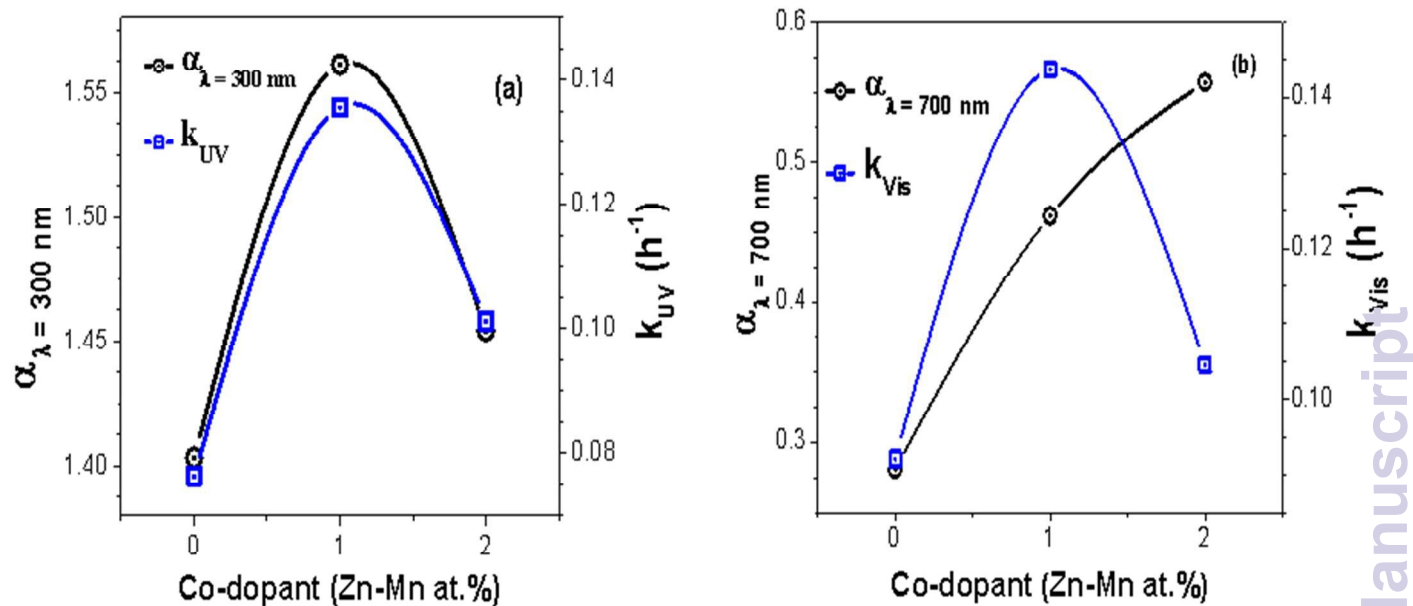


Fig. 13. Correlation between (a) absorbance (α_{λ}) and (b) rate constants (k) for UV and visible radiations. The α_{λ} values for UV and visible radiation were taken at $\lambda = 300$ and 700 nm, respectively.